Journal of the Arkansas Academy of Science

Volume 56 Article 29

2002

Effects of Welding Electropolished Stainless Steel as Used in Ultra-Pure Fluid Delivery Systems for the Semiconductor and Pharmaceutical Industries

Steve Trigwell
University of Arkansas at Little Rock

Guna Selvaduray
San Jose State University

Effects of Welding Electropolished Stainless Steel as Used in Ultra-Pure Fluid Delivery Systems for the Semiconductor and Pharmaceutical Industries

Steve Trigwell*
Applied Science Department
University of Arkansas at Little Rock,
2801 South University Ave
Little Rock, AR 72204
501-569-8067 (ph) • 501-569-8020 (fax)
sxtrigwell@ualr.edu

Guna Selvaduray
Department of Chemical and Materials Engineering
San Jose State University
1 Washington Square
San Jose, CA 95192

* Corresponding Author

Abstract

In the semiconductor and pharmaceutical industries, care is taken to prevent any contribution to product contamination or corrosion from the fluid delivery systems. Electropolished 316L stainless steel has become the industry standard due to its superior corrosion resistance. However, welding of the tubing often leads to discoloration in the heat affected zone (HAZ) which can lead to corrosion. Electropolished specimens from various lots of 316L stainless steel tubing were welded under identical parameters, but with varying concentrations of oxygen leaked into the argon purge gas during the welding, simulating on-site welding conditions. Various levels of discoloration were observed in the HAZ after welding. The chemical composition and thickness of the discoloration and an adjacent clean reference area on each specimen were analyzed by Auger Electron Spectroscopy. The cause of the discoloration was due to an iron-enriched oxide layer in the HAZ in the sensitizing temperature range. The thickness and level of discoloration depended upon the concentration of oxygen in the purge gas. The presence of this oxide layer is due to the rapid growth kinetics of FeO compared to that of Cr_2O_3. The composition of the original steel was found to be only a minor factor in the extent of the discoloration.

Introduction

The purity of chemicals and gases used in the semiconductor and pharmaceutical industries has been subject to heavy scrutiny to minimize contamination, corrosion, or particulate generation. Similarly, the methods of fluid distribution are also now being subjected to the same scrutiny. Due to its superior corrosion resistance and low carbon content (Cormia, 1993), electropolished 316L stainless steel has become the industry standard, especially where extensive welding is to occur. Although strict specifications have been developed (Cormia, 1993) to ensure quality for semiconductor grade tubing, concerns have been expressed by the manufacturers and vendors of tubing regarding the often observed discoloration in the heat affected zone (HAZ) near the weld joint, often referred to as the sensitizing region. Examples of weld zone discoloration on 316L stainless steel are shown in Figures 1 and 2.

Type 316L is used where extensive welding is to occur; it has lower levels of carbon (0.03% max. versus 0.08% for type 316) to reduce the tendency toward carbide precipitation at the grain boundary during welding. In this process, carbon diffuses to the grain boundary in the sensitized region forming chromium carbide precipitates ($Cr_{23}C_6$) which deplete the regions adjacent to grain boundaries of the necessary chromium for passivity.

In order to produce a smooth surface with a uniform chromium-enriched oxide layer that is chemically inert and corrosion resistant, the tubing is subjected to electropolishing and passivation. In electropolishing, iron is selectively removed from the surface, enriching the chromium level. Passivation follows, which oxidizes the surface with a strong oxidizer, usually nitric acid. The resulting finished surface in now smooth and free from machining marks, grooves, and pits, which may be sites for corrosion.

Welding of Type 316L stainless steel is usually performed by pulsed-arc gas tungsten-arc (GTA) welding, also known as tungsten inert-gas (TIG) welding. In the welding process, an arc discharge takes place between the tungsten electrode and the base metal, and metal fusion takes place without the use of a filler. The weld head forms an enclosed chamber that is filled with an inert gas, commonly argon, to protect the molten weld metal from air during the process. Since the welding involves the melting of the base metal itself, the chemical composition of the base metal is important. Variations in difficulty in the weldability

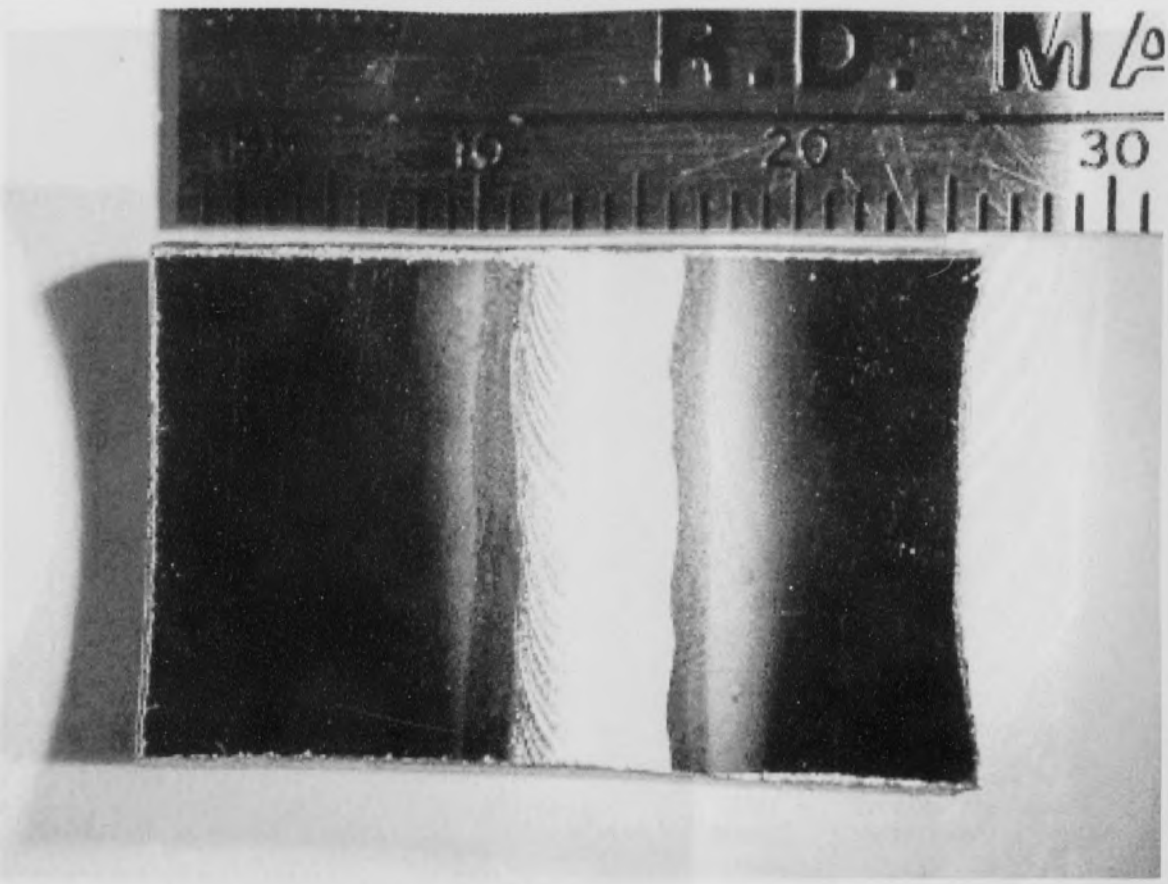

Fig. 1. Example of Heat Affected Zone discoloration on 316L electropolished stainless steel as viewed under a fluorescent lamp.

of different lots of Type 316L have been observed (Burgardt and Heiple, 1986) resulting in deviations of the weld bead from a perfect circle (known as meander) and/or excess discoloration in the HAZ.

Susceptibility to intergrannular corrosion in the HAZ of welded stainless steel has been known for a long time (Uhlig and Revie, 1985) and attributed to the formation of chromium carbide. The low carbon content steels (labeled with an L suffix) were developed to attempt to eliminate this problem. However, work on Types 304L and 316L showed pitting corrosion in the HAZ that was dependant upon the extent to which the HAZ was oxidized (Joshi and Stein, 1972), and increased corrosion in the HAZ when exposed to aggressive gases (HCl, WF_6) that was the result of varying the oxygen leak into the argon purge during welding (Henon and Jekel, 1989). More recent work (Grant et al., 1997) showed the amount of surface etching and pitting was directly proportional to the amount of heat tint present in the HAZ and that the blue ring observed in the HAZ may result from manganese that has been vaporized during welding and redeposited in the HAZ causing preferential corrosion. Other work showed that slight variations in the composition of the alloying elements in Type 316L can have an effect on the welding characteristics (Pollard, 1988) and that there existed variations in the oxide layer thickness and chromium content across the weld zone region, even for no discernable discoloration.

The objectives of this study were therefore to determine the nature of the discoloration in the HAZ and determine exactly how much the extent of discoloration depended upon the composition of the steel.

Materials and Methods

Five different heat lots of 6.35 mm diameter Type 316L stainless steel tubing were used in this study. The lots included a typical "normal" heat (labeled V20892), an Electron Beam Remelt (labeled EBR R3040), a heat lot having a higher than normal tendency to oxidize in the HAZ (labeled Trouble 1 V30110), a heat lot characterized as having severe weld bead meander (labeled Trouble 2 V30112), and a lot with a higher than normal chromium concentration (specified as 16 - 18 wt %) (labeled High Chrome 432958). The elemental bulk compositions of each

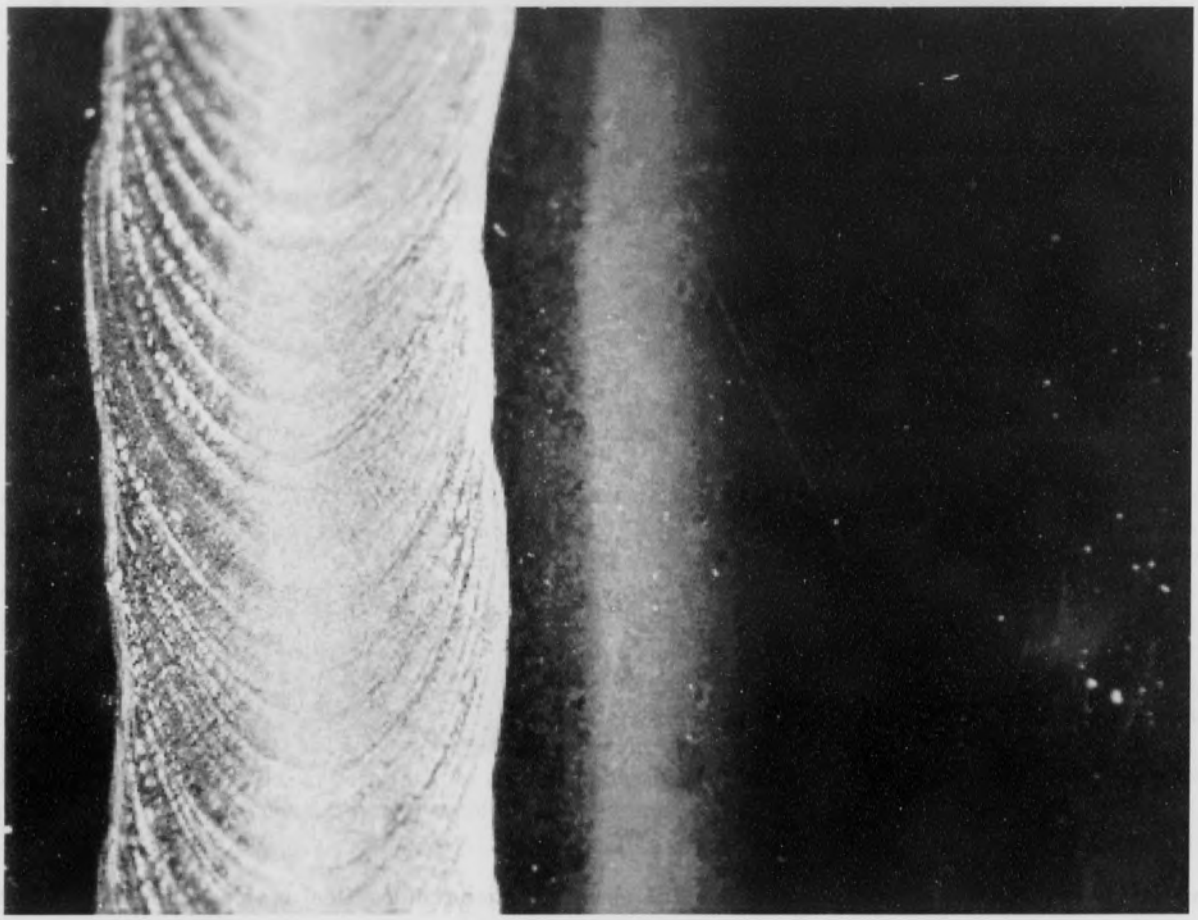

Fig. 2. Higher magnification micrograph showing the discoloration next to the weld zone.

lot as given by the suppliers are shown in Table 1. The welding was performed in a high purity gas fabrication shop at Intel Corporation, Hillsboro, Oregon. A mixing panel was constructed to control accurate ratios of O_2:Ar, and ratios were checked with a Delta-F Platinum Nanotrace O_2 analyzer. A total of 73 runs was performed including runs to establish the welding parameters. After welding, each tube was classified according to the extent of oxidation in keeping with the recommendations in ASTM Standard D1729-96. Acceptability is defined and the weld considered "color free" when no ring is observed when viewed with a fluorescent lamp of know wattage or a 3 volt halogen lamp at a distance of 46 - 61 cm. A sampling plan was established after review of the experiment's objectives with an Intel Corporation statistician (Cohen, 1995 unpub.). A total of 29 welded tubes were chosen for the analysis, covering all the different heats and purge gas levels. The sampling plan is shown in Table 2. The tubes were cleaned with deionized water and dried by blowing cryogenic argon for three minutes through each tube. For the AES analysis, the tubes were cut to approximately ¾ inch in length. Each sample was cut along its axis to expose the inner diameter surface. The cutting was performed using an ultrasonically cleaned, stripped hacksaw blade of fine cut to minimize heat build up in the tubing. The AES experiments were performed on a VG Scientific Microlab 310-F equipped with a field emission source and a background pressure of 10^{-10} torr. The samples were analyzed with an electron beam energy of 10 kV and sample current of 50 nA at a magnification of 10000x. The analysis area was approximately 5 μm square in size. The relative atomic concentrations for each specimen were obtained by measuring the elemental peak-to-peak heights in each spectrum and normalizing with sensitivity factors. The sensitivity factors used in the quantification were obtained from a NIST certified standard of Type 316 stainless steel (SRM 1155). The depth profiles were acquired utilizing an EX05 scanning ion gun using research grade argon ions at an energy of 3 kV, 1 μA, rastered over a 4 mm^2 area. The argon etch rate was calibrated against a thermally grown layer of Ta_2O_5 of 1000 Å thickness on Ta.

Table 1. Bulk elemental compositions of the 316L stainless steel lots as supplied by the vendor

Element Wt. %	Normal V40639	EBR R3040	Trouble 1 V30110	Trouble 2 V30112	High Cr 432958
Carbon	0.020	0.029	0.018	0.017	0.015
Nitrogen	0.010	0.001	---	0.036	0.033
Aluminum	0.002	0.009	0.004	0.004	0.003
Silicon	0.590	0.005	0.400	0.690	0.530
Phosphorus	0.027	0.001	0.024	0.026	0.022
Sulfur	0.009	0.005	0.010	0.011	0.007
Titanium	0.010	---	---	---	---
Chromium	16.490	16.290	16.950	16.640	17.300
Manganese	1.310	0.030	1.510	1.640	1.600
Iron	67.030	66.838	66.174	65.166	63.634
Cobalt	0.030	0.030	0.100	0.150	0.071
Nickel	12.270	14.580	12.480	12.990	14.000
Copper	0.032	0.002	0.280	0.470	0.200
Molybdenum	2.170	2.180	2.050	2.160	2.580

Table 2. Experimental sampling plan. The number of specimens analyzed from each heat lot is indicated.

O_2 content in purge gas (ppm)	Pass/Fail criteria Fluorescent	Maglite	Oxidation level	Normal V40639	EBR R3040	Trouble 1 V30110	Trouble 2 V30112	High Cr 432958
0	Pass	Pass	None	1	2	2	2	2
1.2	Pass	Pass	Light	2	1	NA	NA	2
6.3	Pass	Fail	Medium	2	1	2	2	2
31.6	Fail	Fail	Heavy	NA	NA	2	2	2

The oxide layer thicknesses, defined as the depth at which the oxygen signal falls to half-maximum, are reported as Ta_2O_5 equivalent thicknesses, as accepted by the SEMATECH protocol (SEMASPEC, 1993a). The maximum Cr:Fe ratio was determined in the oxide layer and is used as an indication of the effectiveness of the electropolishing (SEMASPEC, 1993b). Typically this value is greater than 1.5:1 and occurs at about the midpoint of the oxide thickness.

Results

The results of the AES analysis of the surface in the HAZ and reference area of each specimen are reported in Figs. 3 - 12. Each plot shows the relative atomic concentration of a particular element for the reference and HAZ areas of each specimen as a factor of O_2 exposure in the purge gas. The Cr:Fe ratios and oxide layer thickness for each specimen are reported in Figures 13 and 14, respectively.

Discussion

The levels of discoloration optically observed in the HAZ for the various levels of oxygen in the purge gas were similar for all the heat lots. However, there were significant differences detected in the results of the AES data for certain elements among the different heat lots that correlated with the bulk elemental compositions. These differences may have an effect on the long-term corrosion resistance or on the corrosion susceptibility to severely corrosive environments.

The Cr:Fe ratios in the HAZ were on average slightly higher for the high chromium concentration heat lot (432958) and the EBR heat lot (R3040) than the other heats. The relative chromium and iron concentrations in the HAZ were significantly higher in the EBR heat (R3040) for all

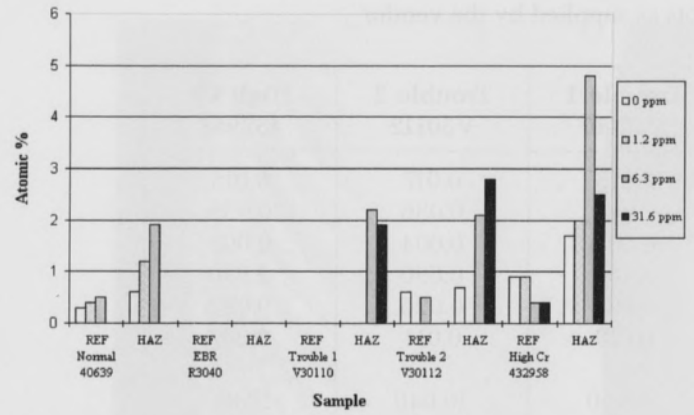

Fig. 3. Silicon concentration variation for different levels of O_2 in weld purge gas.

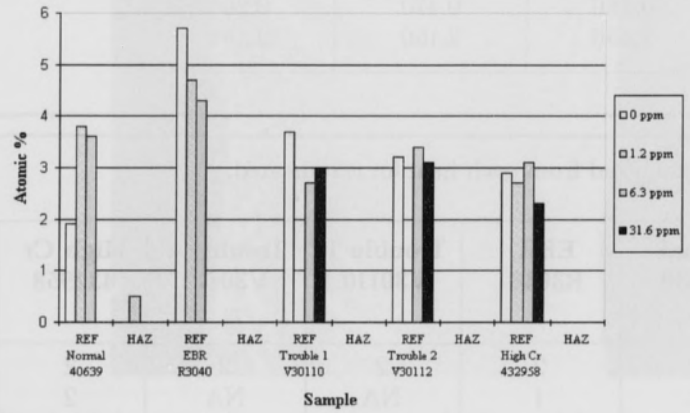

Fig. 4. Phosphorus concentration variation for different levels of O_2 in weld purge gas.

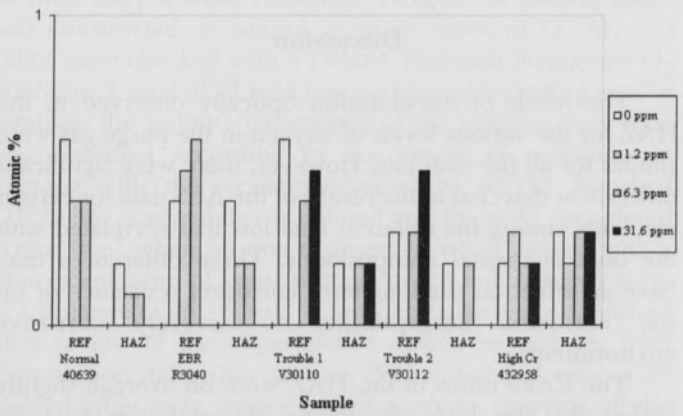

Fig. 5. Sulfur concentration variation for different levels of O_2 in weld purge gas.

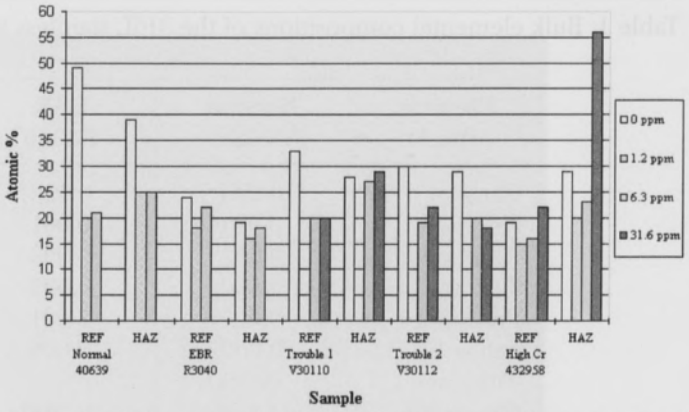

Fig. 6. Carbon concentration variation for different levels of O_2 in weld purge gas.

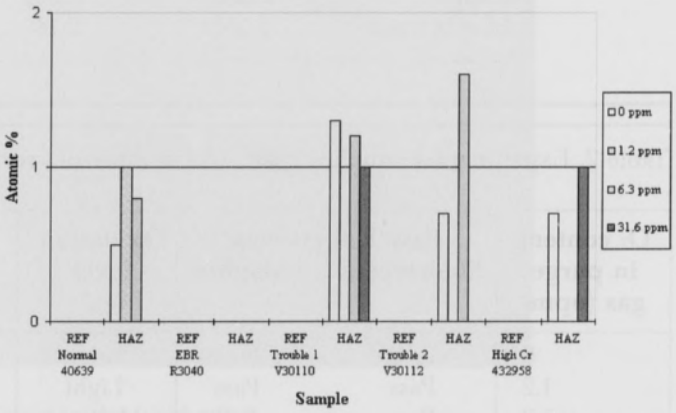

Fig. 7. Tin concentration variation for different levels of O_2 in weld purge gas.

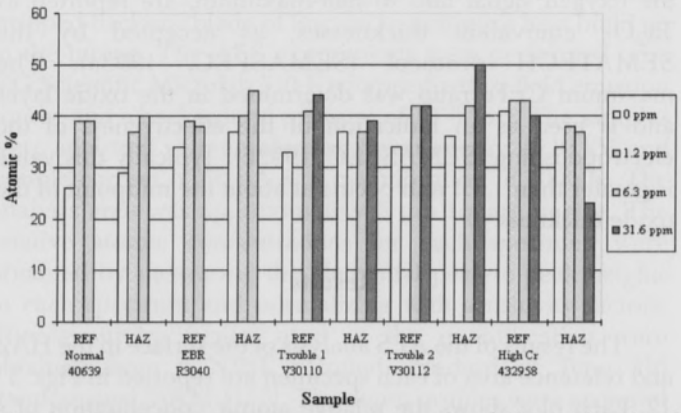

Fig. 8. Oxygen concentration variation for different levels of O_2 in weld purge gas.

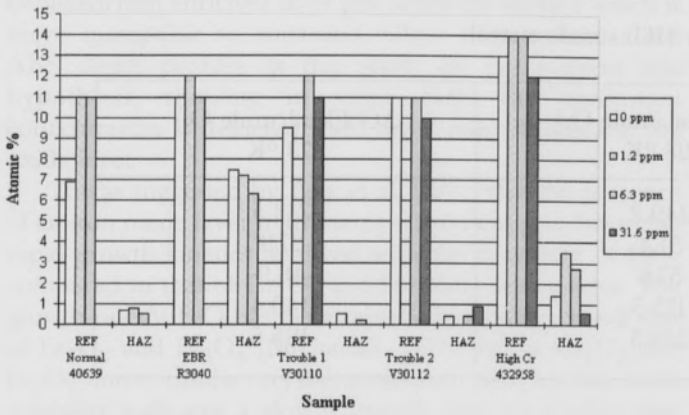

Fig. 9. Chromium concentration variation for different levels of O_2 in weld purge gas.

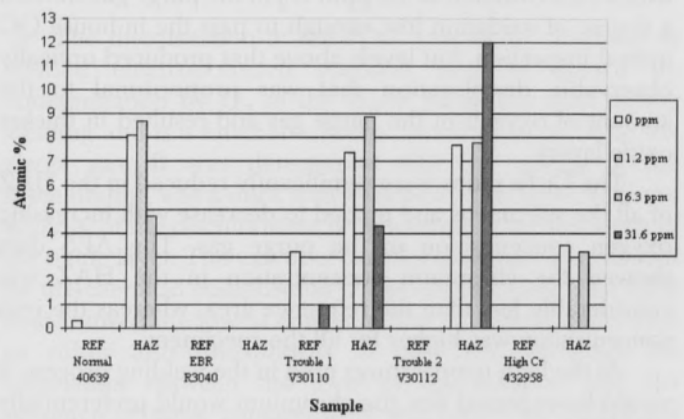

Fig. 10. Manganese concentration variation for different levels of O_2 in weld purge gas.

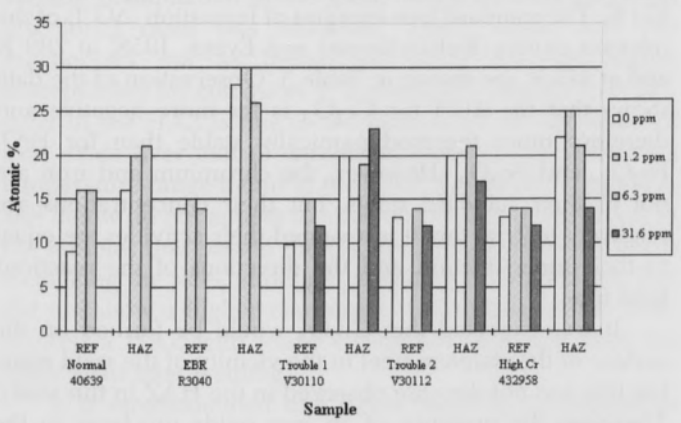

Fig. 11. Iron concentration variation for different levels of O_2 in weld purge gas.

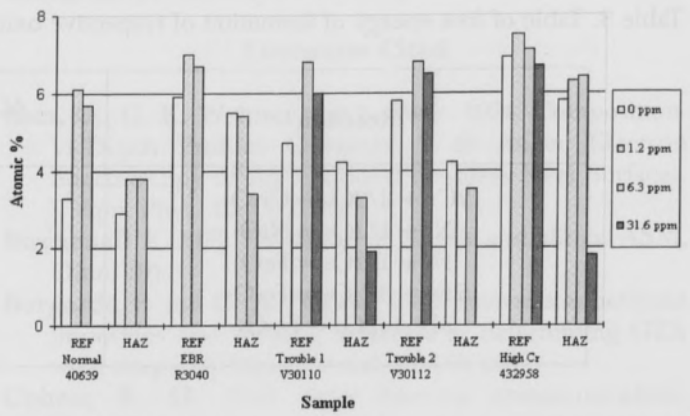

Fig. 12. Nickel concentration variation for different levels of O2 in weld purge gas.

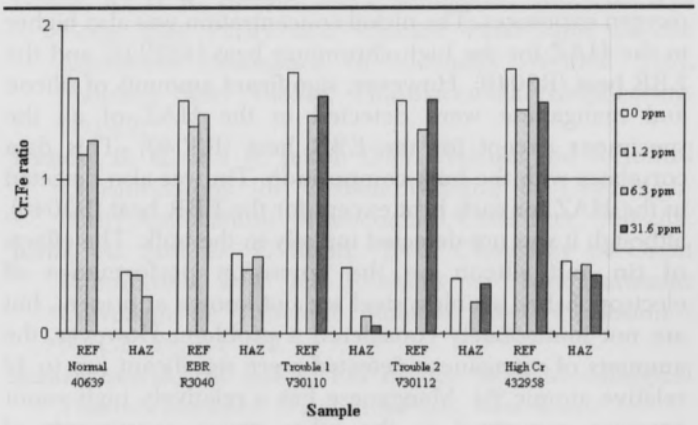

Fig. 13. Cr: Fe ratios for different levels of O2 in weld purge gas.

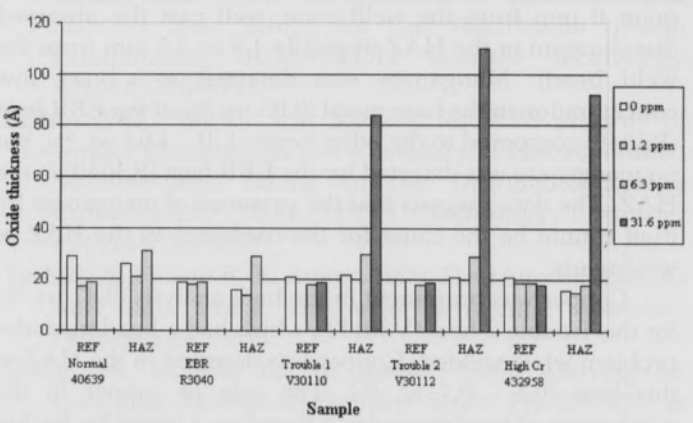

Fig. 14. Oxide layer thickness for different levels of O2 in weld purge gas.

203

Table 3. Table of free energy of formation of respective oxides in 316L stainless steel.

Reaction	ΔG°f(kcal/mole O_2) 298 °K	ΔG°f(kcal/mole O_2) 873 °K
$2Cr + 3/2O_2 = Cr_2O_3$	-249.2	-213.5
$Ni + 1/2O_2 = NiO$	-51.4	-37.9
$Fe + 1/2O_2 = FeO$	-57.6	-48.9
$2Fe + 3/2O_2 = Fe_2O_3$	-175.5	-140.4
$3Fe + 2O_2 = Fe_3O_4$	-238.5	-195.5

oxygen exposures. The nickel concentration was also higher in the HAZ for the high chromium heat (432958) and the EBR heat (R3040). However, significant amounts of silicon and manganese were detected in the HAZ of all the specimens except for the EBR heat (R3040). This data correlates with the bulk composition. Tin was also detected in the HAZ for each heat except for the EBR heat (R3040), although it was not detected initially in the bulk. The effects of tin and silicon on the corrosion performance of electropolished stainless steel are not known at present, but are not immediately considered a problem. However, the amounts of manganese detected were significant (up to 12 relative atomic %). Manganese has a relatively high vapor pressure compared to the other major constituents of stainless steel. AES analyses taken 1 mm apart starting from the edge of the weld zone performed on a specimen of heat lot V30110 with the highest level of discoloration showed the manganese concentration reached a maximum at a point 6 mm from the weld zone, well past the observed discoloration in the HAZ (typically 1.5 to 3.5 mm from the weld bead). Manganese was detected at a very low concentration in the base metal (0.03 wt. %) of the EBR heat (R3040) compared to the other heats (1.31 - 1.64 wt. %), but no manganese was detected for the EBR heat (R3040) in the HAZ. The data suggests that the presence of manganese by itself cannot be the cause for the oxidation in the HAZ of weldments.

Copper was prominent in the bulk analysis (0.47 wt. %) for the Trouble 2 heat (V30112), which had a bead meander problem when welded. Copper was detected in the HAZ of this heat (0.5 - 0.7 at. %). The role of copper in the mechanism of bead meander is therefore a target for further study.

A direct correlation between the amount of discoloration in the HAZ and the amount of oxygen in the purge gas was observed. All of the tested samples welded with a concentration of 1.2 ppm O_2 in the purge gas showed a degree of oxidation low enough to pass the in-house QC optical inspection, but levels above that produced optically observable discoloration that was proportional to the amount of oxygen in the purge gas and resulted in thicker oxide layers.

The Cr:Fe ratios were significantly reduced in the HAZ of all the specimens and tended to decrease with increasing oxygen concentration in the purge gas. The AES data showed the chromium concentration in the HAZ was considerably less than the reference area, whereas the iron concentration was higher for all the specimens.

At the high temperatures used in the welding process, it would be expected that the chromium would preferentially oxidize to form Cr_2O_3 over iron in the vicinity of the weld zone (Kubaschewski and Evans, 1958). Temperature gradient calculations showed the temperature in the vicinity of the HAZ (1.5 – 3 mm from the weld) was approximately 873 K. The standard free energies of formation (ΔG°f) of the relevant oxides (Kubaschewski and Evans, 1958) at 289 K and at 873 K are shown in Table 3. Observation of the data shows that the ΔG°f for Cr_2O_3 is far more negative and therefore more thermodynamically stable than for FeO, Fe_2O_3, and Fe_3O_4. However, the chromium and iron are not in their standard states, but their concentrations are relatively high so that it is assumed their activities are equal to their mole fraction and the directions of the reactions hold true.

It was expected that Cr_2O_3 would be formed on the surface of the stainless steel in the vicinity of the weld zone, but this was not the case observed in the HAZ in this study. Therefore the presence of an iron oxide top layer in the HAZ needs to be explained.

Recent literature (Tuthill and Avery, 1999) proposes that in the sensitized region at this temperature, chromium diffuses to the surface of the metal, leaving a chromium

depleted/iron enriched layer just under the surface which is more susceptible to corrosion. Close examination of the AES depth profiles in this study do not support this hypothesis, showing in some cases the chromium concentration is depleted from the surface throughout the oxide layer.

It was suggested by Betz et al. (1974) that the presence of an iron oxide layer in this temperature range is due to the rapid growth kinetics involved with the formation of FeO, compared to that of Cr_2O_3 and the other iron oxides. The growth rate of FeO has been reported to vastly exceed that of Fe_2O_3 and Fe_3O_4 (Birchenall, 1971) and as Cr_2O_3 and Fe_2O_3 have similar crystal structures and mutual solid solubility indicates a slower growth rate for Cr_2O_3 than FeO. The iron-enriched zone in the HAZ is postulated to be caused by this rapid growth of FeO at the surface.

Conclusions

The discoloration in the HAZ commonly observed in welded electropolished stainless steel is caused by contamination by O_2 of the argon purge gas used during welding and is a function of the concentration of O_2 in the purge gas. It was determined that the nature of the discoloration was a thick iron enriched oxide layer, with the severity of the discoloration proportional to the thickness of the oxide layer. The extent of discoloration was also affected by the chemical composition of the original steel. The EBR heat showed the lowest concentration of contaminants such as sulfur and phosphorus in the bulk, although no correlation between the level of discoloration and the presence of these contaminants was observed. Significant amounts of manganese were detected in the HAZ of all the specimens, although again the level of discoloration was not dependent on the manganese concentration. No evidence of carbide precipitation at the grain boundaries for the worst discolored cases was observed, which would rule this mechanism out as being the cause for the higher susceptibility for corrosion. It is postulated that the iron rich layer in the HAZ is due to the kinetics of the formation of iron oxide over that of chromium oxide in the sensitizing temperature range found in the HAZ. Levels of 1.2 ppm O_2 and below do not appear to affect the degree of oxidation in the samples that passed the QC inspection. Electron Beam Remelting the steel, although producing a composition that did not show a higher chromium composition in the bulk, showed a HAZ with lower chromium depletion than the other heats after welding.

It is recommended that future work be performed to determine if similar results are obtained among other alloys of the Type 300 series and of different alloys.

ACKNOWLEDGMENTS.—The authors would like to thank Mr. Ralph Cohen of Intel Corporation for supplying the tubing and performing the welding.

Literature Cited

Betz, G., G. K. Wehner and **L. Toth.** 1974. Composition-vs-Depth Profiles Obtained With Auger Electron Spectroscopy of Air-Oxidized Stainless Steel Surfaces. J. App. Phys. 45:5312-5316.

Birchenall E. 1971. Oxidation of Metals and alloys. ASM, Ohio. 191.

Burgardt, P. and **C. R. Heiple.** 1986. Interaction between impurities and welding variables in determining GTA weld shape. Welding Journal. 63:150-155.

Cohen, R. M. 1995. Intel Internal communication. Unpublished.

Cormia, R. D. 1993. Super Stainless Steels. Advanced Materials & Processes. 16-20.

Grant, A., B. K. Henon, and **F. Mansfeld.** 1997. Effects of Purge Gas Purity and Chelant Passivation on the Corrosion Resistance of Orbitally Welded 316L Stainless Steel Tubing. Pharmaceutical Engineering. 17:1-22.

Henon, B. K. and **A. Jekel.** 1989. Material and Technical Considerations for Orbital Welding in Ultra-High-Purity Applications. Microcontam. Conf. Proc. 260-284.

Joshi, A. and **D. F. Stein.** 1972. Chemistry of Grain Boundaries and Its Relation to Intergrannular Corrosion of Austenitic Stainless Steel. Corrosion - NACE, 28:321-329.

Kubaschewski, O. and **E. LL. Evans.** 1958. Metallurgical Thermochemistry. Pergamon Press, New York.

Pollard, B. 1988. The Effects of Minor Elements on the Welding Characteristics of Stainless Steel. Welding Journal. 67: 202-205.

SEMASPEC 1993a. Test method for AES analysis of Surface and Oxide Composition of Electropolished Stainless Steel Tubing for Gas Distribution System Components, SEMATECH Transfer Technology #91060573B-STD.

SEMASPEC 1993b. Test Method for XPS analysis of Surface Composition and Chemistry of Electropolished Stainless Steel Tubing for Gas Distribution System Components, SEMATECH Technology Transfer #90120403B-STD.

Tuthill, A. H. and **R. E. Avery.** 1999. Heat tints on stainless steel can cause corrosion problems. Materials Performance. 72-73.

Uhlig, H. H. and **R. W. Revie.** 1985. Alloying for Corrosion Resistance; Stainless Steels. Pp. 297-326, *In* Corrosion and Corrosion Control, J. Wiley & Sons, New York. xiv + 441 pp.